

Thermal Conductivity of Porous Media

Lu Changqing, Mechanical Engineering (2019), *UM-SJTU Joint Institute*

Abstract—Utilizing a computational framework *openBTE*, ballistic limit and diffusive limit are studied for two different models - gray and nongray Si. Both ballistic limit and diffusive limit are dependent on the MFP distribution of the material. To study the parameters that might influence the thermal conductivity at diffusive limit for porous media, several geometries are studied and a possible descriptor - *shape factor* is introduced.

Index Terms—thermal conductivity, porous materials, heat transfer, Boltzmann transport equation, *openBTE*

I. INTRODUCTION

A. Problem Origin

There have been many applications which involve porous materials. For example, We are interested in the thermal conductivity of industrial and civil thermal insulators made by porous materials for energy-saving purposes.

In the microscopic scale, heat is transferred in materials by the collision of phonons. We can think of these phonons as moving particles that transfer energy along their paths. These phonons travel through the material while macroscopically, temperature distribution changes accordingly in the material.

Generally, materials all contains pores of different sizes. Based on the thermal energy transfer mechanism, the phonons will encounter obstacles such as boundaries of different media along their path. The existence of these boundaries will influence the collisions of the phonons when heat is transferred from one end to the other end of a certain material. Therefore, how the pores are arranged in the porous media will strongly influence the thermal conductivity of the porous media.

B. Method

Based on the research of Giuseppe Romano and Jeffrey C. Grossman [1], a computational framework, *openBTE*, is developed based on the *Boltzmann transport equation* to solve thermal transport problem in nano-structured materials of any geometry with bulk cumulative thermal conductivity as the only input. This method is less time-consuming while still remains accuracy when it is compared to the solution gained from solving the frequency-dependent Boltzmann transport equation.

The idea of *openBTE* for solving certain geometry is that by discretization of mean free path (MFP) of a material, a *suppression function* is developed for each mean free path range for a certain geometry. The *suppression function* is a quantified description of the influence of the geometry (arrangement of pores in the material) on the contribution of the mean free path to the total thermal conductivity of the material.

Therefore, by generating certain geometry and material properties as input to the solving framework, we are able to solve the thermal conductivity of the material with porous structure.

II. VALIDATION

To validate the calculation of *openBTE* framework, both gray and nongray Si with bulk geometry are calculated first.

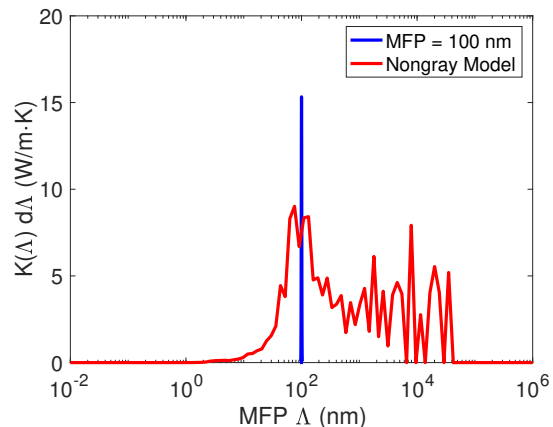


Figure 1: Mean free path distribution: nongray and gray model of Si

Figure 1 shows the distribution of mean free path of Si in gray and nongray model. As we can see the gray model has a single mean free path of 100 nm. And the nongray Si has a distribution with data provided by the *openBTE*. The distribution shows the contribution of each phonon mean free path to the total thermal conductivity of the material.

Therefore, by the idea of *openBTE*, we can calculate the cumulative bulk thermal conductivity by interacting the distribution function,

$$\kappa = \int_0^\infty S(\Lambda)K(\Lambda)d\Lambda \quad (1)$$

where Λ is the mean free path, $K(\Lambda)d\Lambda$ is the contribution of the mean free path Λ and $S(\Lambda)$ is the suppression function.

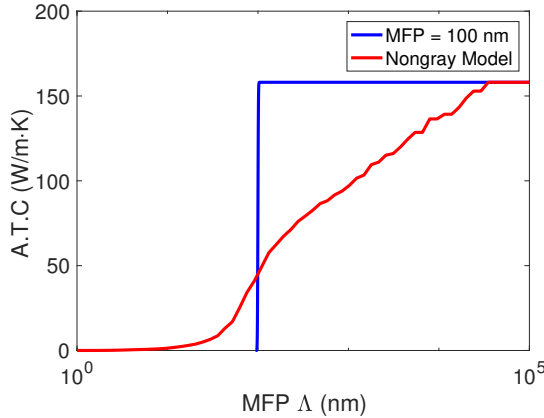


Figure 2: Accumulative thermal conductivity: nongray and gray model of *Si*

As we can see from Figure 2, when integrating over all the phonon mean free path of the material, the total thermal conductivity of *Si* of both gray and nongray model is $\kappa_{Si} = 158.074 \text{ W/m} \cdot \text{K}$. And this results confirms the calculation results of the *openBTE* for bulk case, where for bulk geometry with no pores, the *suppression function* equals to 1.

The following results and discussions are all based on these two models: nongray model of *Si* and gray model of *Si* with single MFP of 100 nm.

III. MEAN FREE PATH OF MATERIALS

A. Heat Transfer Mechanism

Thermal energy is transferred in the media by collisions of phonons. Within a certain material, generally, there are phonons with a wide distribution of mean free paths. Recall that mean free paths are the average distance that a phonon can travel without colliding with another.

1) *Ballistic Limit*: When the size of the pores (L_c) are comparable with or even smaller than the MFPs of the phonons, the ballistic limit of heat transfer is reached since it is highly possible that a phonon pass the material without any collisions with other phonons, resulting in ineffective heat transfer.

2) *Diffusive Limit*: When the size of the pores (L_c) are much greater than the MFPs of the phonons, diffusive limit is reached where the pores are considered macroscopic. Within the solid media, we can simply use diffusive solutions because phonons will experience multiple collisions when traveling through the media.

3) *MFP Distribution*: As discussed in the previous section, the relative size between the characteristic length of the material (L_c) and the MFP (Λ) will influence the thermal conductivity of the material.

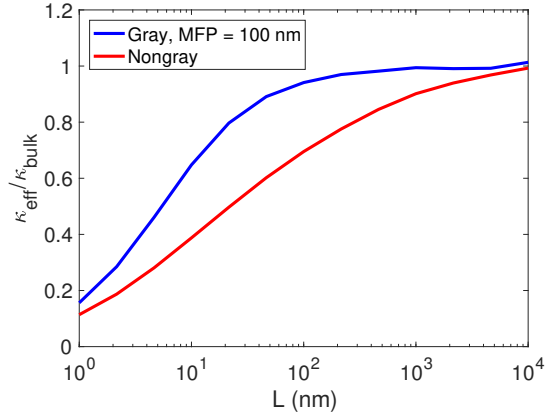


Figure 3: Ballistic to diffusive limit for nongray and gray model of *Si*, Bulk

As we can see from Figure 3, for bulk *Si* material, when the model is gray, the diffusive limit is reached when the characteristic length of the material is approximately $L \approx 100 \text{ nm}$, which is the MFP of the model. For nongray model, we can see that when approximately $L = 10^4 \text{ nm}$, the diffusive limit is reached. Recall Figure 1 for nongray model, we can see that there are MFPs greater than 10^4 nm that contribute to the thermal conductivity. Therefore, we can conclude that the characteristic length of diffusive limit for a certain material depends on the largest MFP that contributes to the thermal conductivity.

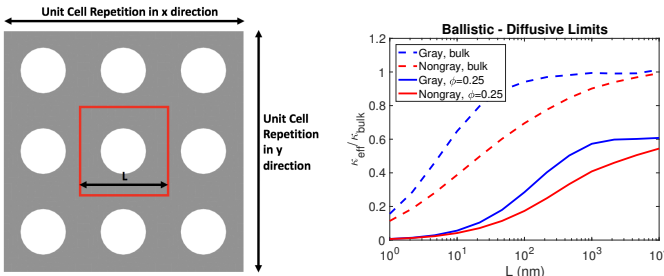
IV. UNIFORM DISTRIBUTION OF PORES

In reality, the arrangement of pores in solid media can be complicated because of the variation of pore shape, pore size and position. To investigate the possible parameters of porous media that influence the thermal conductivity, we should start with simple geometries.

A. Circular Pores

For circular pores in a square lattice (Figure 4a), we first investigate the ballistic and diffusive limit of this configuration. The given geometry has a porosity (φ) of 0.25, where porosity is the volume (3D) or area (2D) ratio between the pores and the bulk. Figure 4b shows the ballistic and diffusive limit for the corresponding geometry shown in Figure 4a.

Note that for the configuration, we have assigned a temperature difference between the left and right boundary of the unit cell by $\Delta T = 1 \text{ K}$.



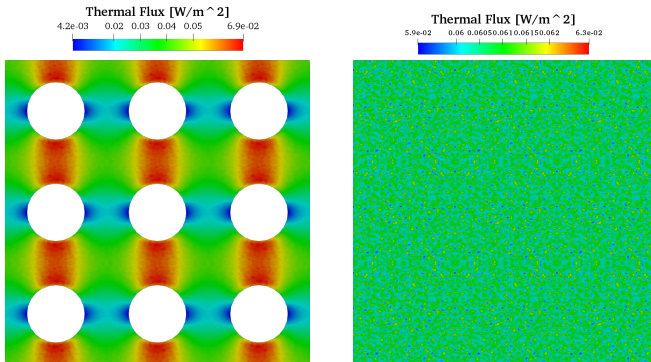
(a) Geometry: square lattice with circular pores, porosity $\varphi = 0.25$, unit cell size = L .

(b) Ballistic to diffusive limit of circular pores with porosity $\varphi = 0.25$ compared to bulk geometry.

Figure 4: Circular pores with $\varphi = 0.25$.

From Figure 4b, we can see that when the unit cell size is the same, the porous material has lower thermal conductivity than the bulk material. This makes sense because the porous geometry has suppression effect on the thermal conductivity based on the previous analysis.

We can see that when the unit cell size $L \approx 10^3$ nm, the gray model of Si reaches its diffusive limit. Compared to the bulk geometry with $L \approx 100$ nm to reach diffusive limit, we can conclude that the porous geometry has influenced the distribution of phonon heat transfer path. This change of path distribution can be shown by a comparison of thermal flux distribution of two geometry.



(a) Thermal flux distribution of square lattice with circle pores.

(b) Thermal flux distribution of bulk.

Figure 5: Thermal flux distribution

Due to the existence of pores, thermal flux distribution is not uniform while for bulk, thermal flux is uniform (Figure 5). We can see high thermal flux between the pores, which means that the phonons collisions happen more frequently in these regions. Therefore, we can conclude that the existence of these pores changes the paths phonons travel in the materials, resulting in a decrease in thermal conductivity.

Since from Figure 5a, we can see thermal flux largely increases in the region between pores in y direction and decreases a little between pores in the x direction.

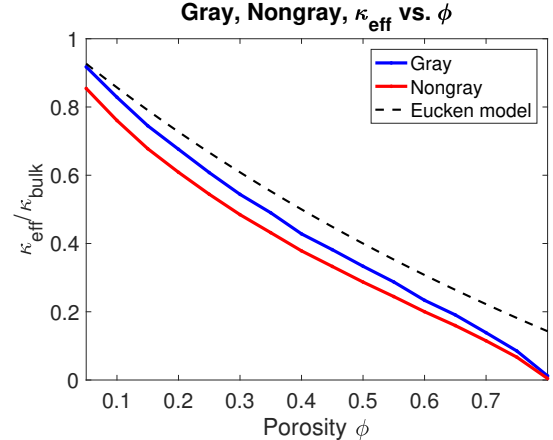


Figure 6: Thermal conductivity vs. porosity for nongray and gray model with unit cell size $L = 10^4$ nm.

By changing the porosity of the geometry (Figure 6), we can see with increase in porosity, the *effective thermal conductivity* κ_{eff} decreases for both models. At the same porosity, gray model has higher thermal conductivity because it is closer to diffusive limit than the nongray model.

Compared with the *Eucken model* which describes the circular porosity and thermal conductivity relationship as

$$\kappa_{\text{eff}}/\kappa_{\text{bulk}} = \frac{1-\varphi}{1+\varphi/2}, \quad (2)$$

we can see that the results from *openBTE* agrees with the model with some differences. The differences might be caused by the discretization of the geometry within the computation framework. Since as the porosity increases, the distance between the boundaries of the circular pores will decrease. As a result, the geometry between the boundaries will require finer discretization to maintain a certain accuracy but this will increase the computation to a large extent, which is unnecessary in the scope of our study.

B. Elliptic Pores

We have discussed the circular porous geometry, which are rotational symmetric. We now consider a less symmetric porous geometry - square lattice with elliptic pores.

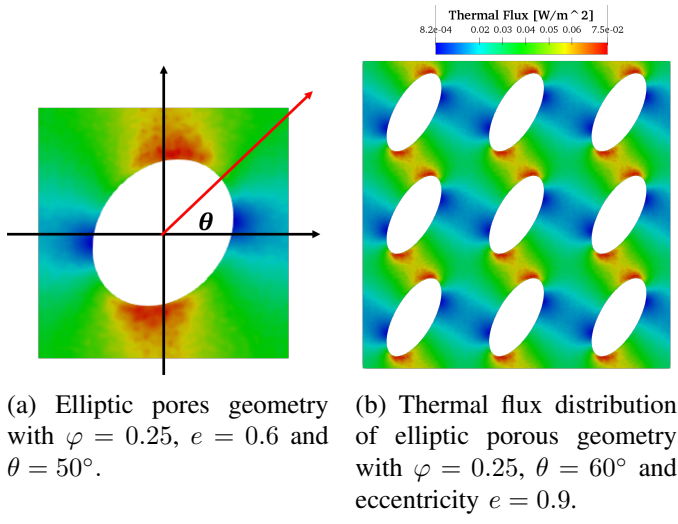
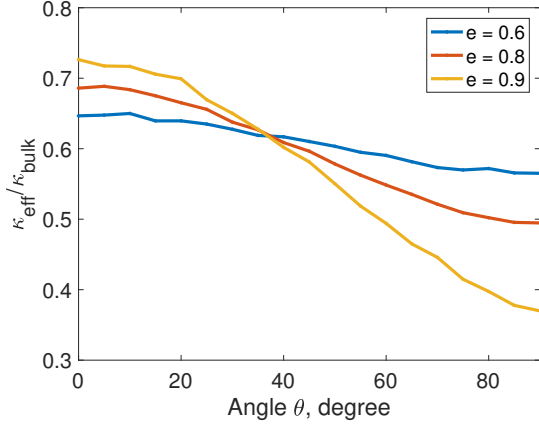


Figure 7: Elliptic pores geometry

Figure 7b is an example of the porous geometry being investigated. The ellipse pores are arranged in the center of the square lattice with an eccentricity of $e = 0.9$ and a porosity of $\varphi = 0.25$, and the ellipse has rotated from the x axis by an angle of $\theta = 60^\circ$. By changing both the eccentricity and the angle θ , we can study the relationship between the parameters and the thermal conductivity. For example, for geometry like Figure 7b, $\kappa_{eff}/\kappa_{bulk} \approx 0.5$.

Figure 8: Thermal conductivity of elliptic pores with $\varphi = 0.25$, gray model with MFP = 100 nm.

At the same eccentricity e , we can see a decreasing trend in the thermal conductivity κ_{eff} as the angle θ increases. From Figure 7b, we can see that when θ increases, the elliptic pores will narrow the path that the phonons can travel through the material. Compared to Figure 5a, the thermal flux has a greater range for the elliptic pores configuration. At the tip of the ellipse, higher thermal flux is observed and between the tilting ellipses because more phonons will be colliding with the

boundaries since there are less paths to travel through. Lower thermal flux is observed because it is more difficult for the phonons to travel in those regions.

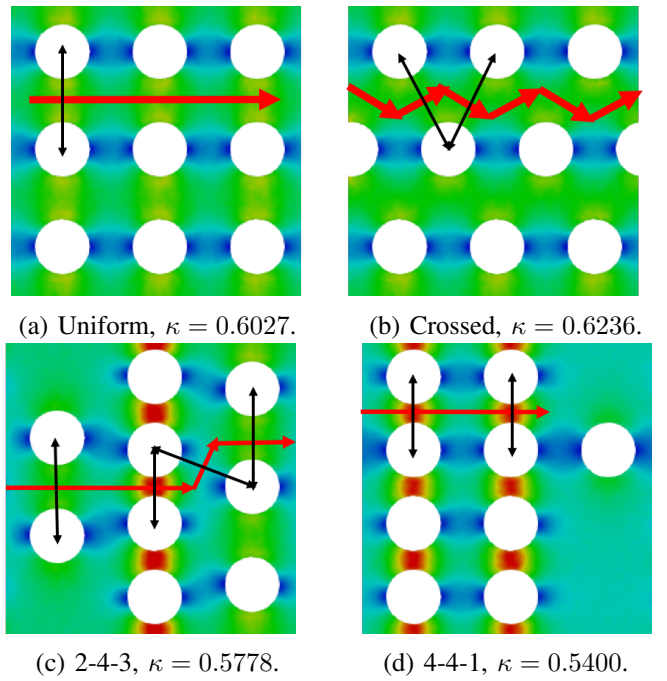
As the eccentricity e increases, the difference between elliptic pores with small θ and large θ increases. This is because with lower eccentricity, as the elliptic pores turns an angle θ , the paths for the phonons to travel decreases less quickly. As eccentricity further decreases to $e = 0$, we have circular pores again. Therefore, we can predict that the curves in Figure 8 converges to a horizontal line with $\kappa_{eff}/\kappa_{bulk} \approx 0.6$.

V. RANDOM DISTRIBUTION OF PORES

Up to this point, we have discussed square lattice with single pores at porosity $\varphi = 0.25$. These pores are uniformly distributed within the geometry. Now we want to study the cases where there are multiple pores within one unit cell, where these pores have relatively random distribution.

A. Square Lattice Distribution

Based on the uniformly distributed 9-pore geometry (Figure 9a), positions of the pores are changed so that the geometry becomes less organized. Note that for all the following geometry, porosity is unchanged ($\varphi = 0.25$) and the size of all the pores are the same.

Figure 9: Thermal conductivity of four geometry, where $\kappa = \kappa_{eff}/\kappa_{bulk}$. Red arrows indicates the possible paths that phonons can travel along, and black lines indicate the planes that are normal to the paths.

From four geometries in Figure 9, we have the highest thermal conductivity for crossed configuration (Figure 9b) and lowest thermal conductivity for the 4-4-1 pore configuration (Figure 9d). We can explain this thermal conductivity difference by the difference in suppression effect by the geometry on the possible paths that phonons can travel along.

Since there are two four-pore columns in 4-4-1 configuration, it is the most difficult geometry for phonons to pass through, resulting in the lowest thermal conductivity.

Comparing uniform and crossed configurations, we can see that the crossed geometry has a higher thermal conductivity. This can be explained by Figure 9b. We can see that the phonons possibly travel through the geometry in zigzag paths. Normal to these paths, the cross section area of the crossed configuration is larger compared to the uniform configuration, allowing more phonons to travel through easily.

Comparing uniform and 2-4-3 configuration, we see that 2-4-3 configuration has lower thermal conductivity. This shows that it is the four-pore column that has the strongest constraint on the thermal conductivity.

B. Shape Factor

It is clear that the properties of the porous geometry will influence the thermal conductivity. Therefore, we introduce *shape factor* to better describe the geometry. Shape factor for a certain geometry is calculated by

$$\frac{1}{s.f.} = \int_0^1 \frac{1}{A(x)} dx, \quad (3)$$

where $A(x)$ is the cross section area that is occupied by the material (See Figure 10a).

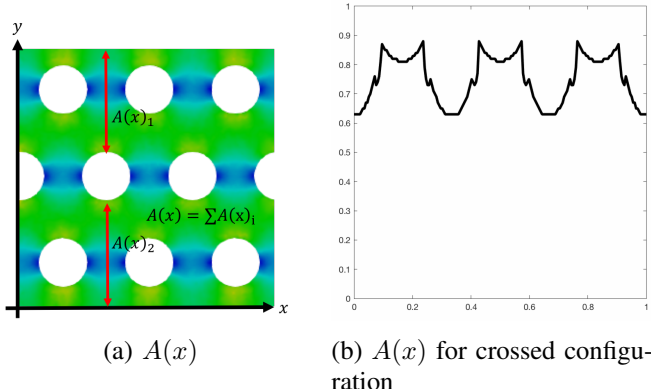


Figure 10: Shape Factor

By this definition, we can calculate the shape factor for the above geometry in Figure 9. For a 2-4-3 geometry,

$$s.f._{2-4-3} = 0.6297,$$

while for a 4-4-1 geometry,

$$s.f._{4-4-1} = 0.5817.$$

We can see that the geometry with a higher shape factor, the thermal conductivity is also higher.

C. Random Square Lattice Distribution

Based on the geometry in Figure 9a, we now randomize the position of the nine pores to a certain extent and calculate the thermal conductivity.

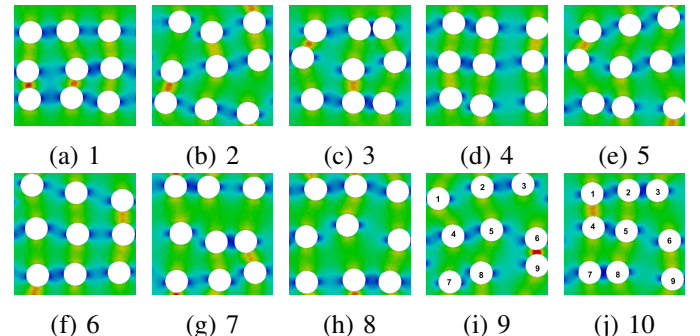


Figure 11: Thermal flux of 10 random 9-pore geometry.

As we can see from Figure 11j, by changing the center position of the circular pores, thermal flux distribution is changed accordingly as a result. Note that we have some uniform thermal flux distribution such as Figure 11d and Figure 11h while we also have some high thermal flux case such as Figure 11i and Figure 11a. The thermal conductivity results for diffusive limit for these geometries are shown in the following figure.

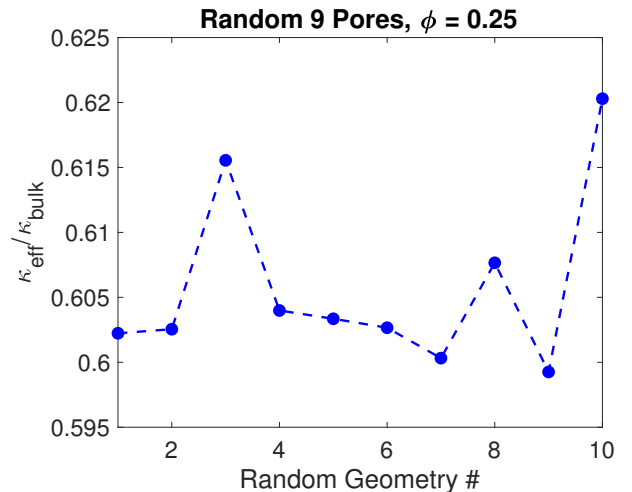


Figure 12: Thermal conductivity of 10 nine-pore-random geometries.

Note that the results (Figure 12), geometry 10 has the highest thermal conductivity. Referring to the geometry

(Figure 11j), we can see that between each row of the pores, the cross section area that allows the phonons to travel through is relative larger than other geometry. Note that geometry 9 (Figure 11i) has the lowest thermal conductivity. This is caused by a small distance between pore #6 and pore #9.

According to the definition of the shape factor, we also calculated their shape factor.

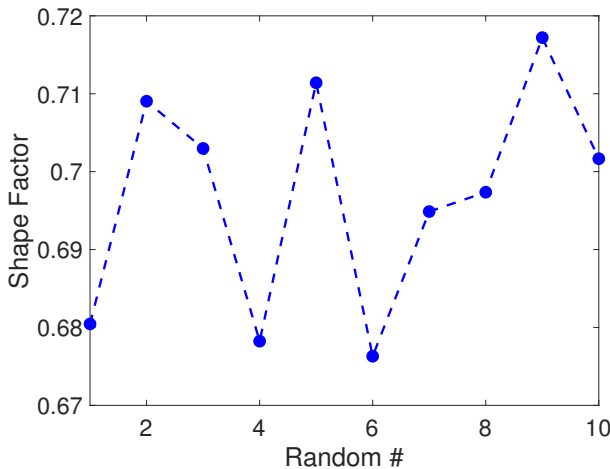
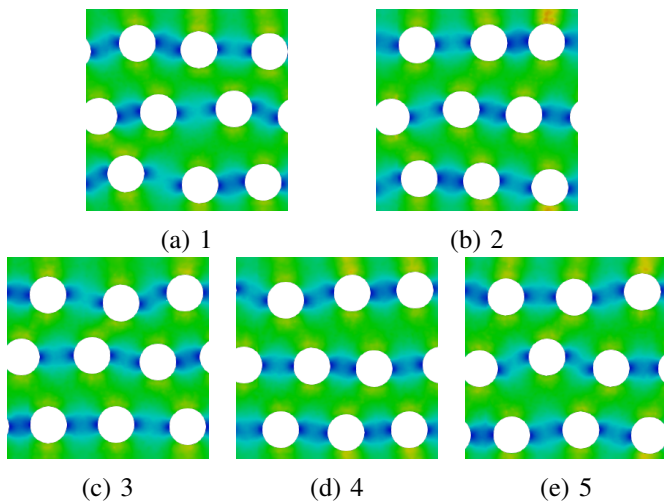


Figure 13: Shape factor of 10 random geometries.

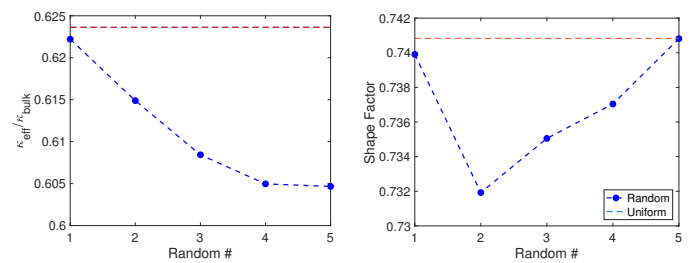
Compare between Figure 12 and Figure 13, we can see that when comparing between some geometries, the shape factor is high for high thermal conductivity geometry. But there are cases where higher shape factor results in lower thermal conductivity. Therefore, the shape factor under our definition can not fully describe the influence of random pore geometry on thermal conductivity.

D. Random Crossed Distribution

Based on the geometry in Figure 9b, we randomized the position of the pores to study the thermal conductivity. The randomized geometry cases are shown below.



For these geometries, both thermal conductivity κ_{eff} and the shape factor are all calculated. (Figure 15)



(a) Thermal conductivity.

(b) Shape factor.

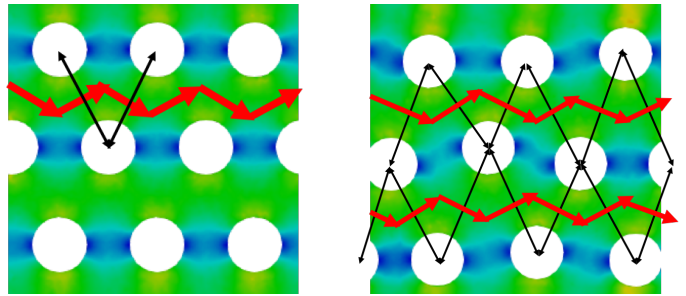
Figure 15: Five cross and randomized geometry.

Compare the thermal conductivity and the shape factor results. We can see that all of the five random geometries have lower κ_{eff} and shape factor than the uniformly crossed one. But when comparing within the random geometries, the relationship between shape factor and thermal conductivity becomes unclear.

VI. DISCUSSION

A. Thermal flux in random porous geometry

Compare how phonons pass through the geometries for uniformly crossed one and random geometry #5, we can see that both of the geometries have approximately the same shape factor by the definition in Equation 3 but random #5 has a much lower thermal conductivity.



(a) Uniformly crossed.

(b) Random #5.

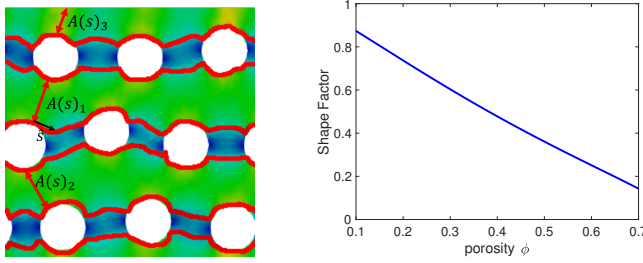
Figure 16: Thermal flux distribution for uniformly crossed geometry and random #5.

In both Figure 16b and Figure 16a, possible phonon travel path is shown. We can see that for random #5, there should be three different paths due to the randomized pore position while for uniformly crossed geometry, there are three identical paths. Phonons travel normal to the cross section areas between pores that are indicated by the black arrows. Since the paths for phonons to travel are not the same between uniformly crossed geometry and random #5 geometry, we should expect different

thermal conductivities. Therefore, the shape factor we defined is not fully descriptive.

B. Proposed shape factor correction

The proposed correction for calculating the shape factor is to generalize $A(x)$ in Equation 3. Since heat flow does not necessarily travel perpendicular to y direction, we should generalize $A(x)$ to be $A(s)$ that calculate the area with material that is perpendicular to the direction of the heat flow (Figure 17a).



(a) Proposed shape factor definition correction. (b) Shape factor vs. single circular pores porosity ϕ .

Figure 17: Shape Factor Correction

The correction that requires $A(s)$ to be perpendicular to the heat flow is that when we are clear that heat flow travels along the $+x$ direction, the shape factor can be descriptive about the thermal conductivity relationship (Figure 17b). Compare the results of thermal conductivity of single circular pores with variation of porosity in Figure 6, we can see that the shape factor and the thermal conductivity follows the same decreasing trend when porosity increases.

VII. CONCLUSION

Based on the results of thermal conductivity for different porous geometry, several conclusions can be made.

- 1) At ballistic limits, the porous geometry will have a suppression effect on the contribution of each MFP band to the total thermal conductivity.
- 2) For a certain material, the characteristic length that will reach diffusive limits is based on the largest MFP that contributes to thermal conductivity of the material.
- 3) Shape factor is descriptive about the thermal conductivity of a certain type of porous geometry, where the $A(x)$ is perpendicular to the direction of the heat flow. Further correction is needed if one wants to use shape factor to fully describe thermal conductivity of a random porous geometry.

REFERENCES

- [1] Romano G, Grossman JC. *Heat Conduction in Nanostructured Materials Predicted by Phonon Bulk Mean Free Path Distribution*. ASME. J. Heat Transfer. 2015;137(7):071302-071302-7.
- [2] G. Romano and A. M. Kolpak, *Directional phonon suppression function as a tool for the identification of ultralow thermal conductivity materials*, Sci. Rep. 7, 44379, 2017.

APPENDIX A OPENBTE FLOWCHART

There are two basic parts to specify in order to get a solution from the framework, namely the *Geometry* and the *Material*. In the *python* package of *openBTE*, there is preset simple geometries and a material file *Si-300K.dat* which describes the MFP distribution of *Si* and 300 K.

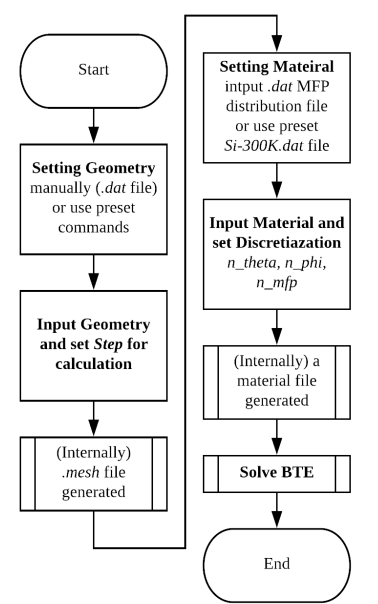


Figure 18: openBTE Flowchart

APPENDIX B OPENBTE DISCRETIZATION

For results that converge, n_{theta} , n_{phi} , and $step$ should be set appropriately for different characteristic length L .

	$\sim 10 \mu m$	$\sim 1 \mu m$	$\sim 100 \mu m$
n_{phi}	~ 80	40	40
n_{theta}	8	40	40
$step$	$\sim L/40$	$\sim L/50$	$L/80$

Table I: openBTE discretization setting